Nano Energy (2014) 6, 193–199

Available online at www.sciencedirect.com

ScienceDirect

journal homepage: www.elsevier.com/locate/nanoenergy

RAPID COMMUNICATION

Porous $ZnMn_2O_4$ microspheres as a promising anode material for advanced lithium-ion batteries

Nana Wang[a], Xiaojian Ma[a], Huayun Xu[a], Liang Chen[a], Jie Yue[a], Feier Niu[a], Jian Yang[a,*], Yitai Qian[a,b,**]

[a]*Key Laboratory of Colloid and Interface Chemistry, Ministry of Education School of Chemistry and Chemical Engineering, Shandong University, Jinan 250100, PR China*
[b]*Hefei National Laboratory for Physical Science at Microscale, Department of Chemistry, University of Science and Technology of China, Hefei 230026, PR China*

Received 8 March 2014; received in revised form 4 April 2014; accepted 8 April 2014
Available online 18 April 2014

KEYWORDS
Transitional metal oxides;
Porous structure;
Li-ion battery

Abstract
High-quality porous $ZnMn_2O_4$ microspheres composed of interconnected nanoparticles have been achieved by calcination of metal carbonates synthesized by a solvothermal reaction. The porous microspheres are characterized by XRD patterns, SEM, TEM, and HRTEM images to reveal the crystal phase and particle morphology. The porous structure and nanoscale building blocks of $ZnMn_2O_4$ microspheres make them a promising anode material for lithium ion batteries. After 300 cycles at a current density of 500 mA g^{-1}, they still preserve a reversible capacity of 800 mAh g^{-1}. Even at 2 A g^{-1}, the reversible capacity could be 395 mAh g^{-1}, higher than the theoretical capacity of graphite. The superior electrochemical performances can be associated with the porous structure and nanoscale building blocks, which promote the contacting between electrolyte and electrode, accommodate volume change during discharge/charge processes, and provide a large number of active surface sites for lithium storage.

Introduction

Nowadays, rechargeable Li-ion batteries (LIBs), as one of the most important devices for energy storage, have enjoyed a great commercial success in portable electronics [1–3]. But the electrode materials could not satisfy the

*Corresponding author. Tel.: +86 531 63606804.
**Corresponding author at: Hefei National Laboratory for Physical Science at Microscale, Department of Chemistry, University of Science and Technology of China, Hefei 230026, PR China. Tel.: +86 551 63606804.
E-mail addresses: yangjian@sdu.edu.cn (J. Yang), ytqian@ustc.edu.cn (Y. Qian).

http://dx.doi.org/10.1016/j.nanoen.2014.04.001
2211-2855/

needs of high-energy applications like electric vehicles. So, a variety of transition metal oxides have been widely investigated as potential electrode materials for advanced LIBs, due to their outstanding reversible capacities and widespread availability [2-5]. Ternary $ZnMn_2O_4$ with a spinel-like structure is attractive, because of its low-cost, high abundance of Zn and Mn, low toxicity to environment, low working potential and high energy density [6]. Moreover, the lithium storage process of this material involves both conversion reactions and lithiation alloying, leading to a theoretical capacity of 1024 mAh g^{-1} [7].

However, large volume changes during discharge/charge processes would easily lead to the smash of anode materials and thus cause rapid degradation upon the cycling [2]. Thus, intensive efforts have been devoted to the development of novel nanostructures, because nanostructured materials could greatly shorten the diffusion distance of lithium and reduce the volume change during discharge/charge processes. $ZnMn_2O_4$ nanocrystals in size of 30-60 nm showed a reversible capacity up to 569 mAh g^{-1} at a rate of 100 mA g^{-1} after 50 cycles [8]. The lithium-storage performance could be increased to 650 mAh g^{-1} at 100 mA g^{-1} after 40 cycles by $ZnMn_2O_4$ nanowires prepared by a solid-state reaction between alfa-MnO_2 nanowires and $Zn(Ac)_2$ [9]. Compared with the two cases, $ZnMn_2O_4$ nanoplate assemblies obtained by calcination of metal-organic nanoparticles only exhibited a specific capacity of 502 mAh g^{-1} at 60 mA g^{-1} over 30 cycles [10]. Lou et. al. reported a coprecipitation-calcination process for hollow $ZnMn_2O_4$ microspheres composed by tiny nanoparticles [11]. The microspheres delivered a specific capacity of 607 mAh g^{-1} at a current density of 400 mA g^{-1} after 100 cycles, due to the presence of hollow structures. Later, the same group developed a similar method to double-shell $ZnMn_2O_4$ hollow microspheres by heating hollow metal glycolate microspheres in air [12]. The cycling performance was further improved to 750 mAh g^{-1} at 400 mA g^{-1} over 120 cycles. However, these capacities are still lower than its theoretical capacity [6,8-14].

In this work, porous $ZnMn_2O_4$ microspheres (ZMO-MSs), not hollow microspheres, are prepared for the first time, which are achieved by a solvothermal synthesis and then a calcination process. Compared with hollow microspheres, the porous ones could apparently increase the packing density of electrode material, benefiting the lithium-storage performance in practical applications [15,16]. Meanwhile, a plenty of pore spaces in this structure effectively tolerate volume variation during discharge/charge processes and allow liquid electrolyte to easily diffuse into active materials. Its high surface area provides good interface contact between electrode and electrolyte [15-17]. All these features make porous ZMO-MSs promising in LIBs, which is supported by their specific capacity of 800 mAh g^{-1} after 300 cycles at a rate of 500 mA g^{-1}. To the best of our knowledge, it is one of the best performances for ZMO as an anode. The superior rate capability is also demonstrated for porous ZMO-MSs.

Experimental section

Synthesis

$MnCl_2 \cdot 4H_2O$ (0.396 g), $ZnCl_2$ (0.613 g) and urea (0.300 g) were dissolved in 40 mL of ethylene glycol. Then, the solution was transferred into a clean Teflon-lined autoclave. After the autoclave was heated to 200 °C for 24 h, the product was collected by filtration and washed with deionized water and ethanol several times, followed by drying in vacuum at 60 °C. Finally, the sample was calcined at 600 °C for 2 h in air to produce ZMO-MSs.

Structural characterization

X-ray powder diffraction (XRD) patterns of the samples were achieved on a Bruker D8 advanced X-ray diffractometer ($Cu_{k\alpha}$ radiation, λ=1.5418 Å). TEM images and FESEM images were obtained from a transmission electron microscope (JEM-1011) and a field-emission scanning electron microscope (JEOL-JSM-6700F), respectively. HRTEM images were observed on a high resolution transmission electron microscope (HRTEM, JEOL-2011) operating at 200 kV. Thermal gravimetric analysis (TGA) for the samples was recorded in air on a Mettler Toledo TGA/SDTA851 thermal analyzer. The chemical composition of the products has been analyzed by Inductive Coupled Plasma Atomic Emission Spectrometer (ICP-AES, IRIS Inrtrepid II XSP). Nitrogen sorption isotherm was examined on a Micromeritics ASAP-2020HD88 instrument.

Electrochemical measurements

Electrochemical performances of ZMO-MSs were tested in 2032-coin cells. To fabricate the working electrode, ZMO-MSs (75 wt%), conductive carbon black (15 wt%) and sodium carboxyl methyl cellulose (CMC, 10 wt%) were dispersed in deionized water and ball-milled (QM-3SP2 Planetary Ball Mill) for 2 h. The resulting slurry was then coated on a Cu foil, resulting in a thin film with a thickness of 200 μm. After drying under vacuum at 80 °C for 12 h, the typical loading density of the active material was in the range of 1.5-2.0 mg cm^{-2}. The cells were assembled in an argon filled glovebox (Mikrouna, Super 1220/750/900) with lithium metal as an anode, Celgard 2400 microporous membrane as a separator, and a solution of 1 M $LiPF_6$ in mixture of ethylene carbonate (EC), diethyl carbonate (DEC) and dimethyl carbonate (DMC) (1:1:1, volume ratio) as an electrolyte. Galvanostatic discharge-charge cycling was performed on Land-CT2001A battery cyclers (Xinnuo, Wuhan China) at room temperature. Cyclic voltammograms (CVs) were tested by a LK-2005A electro-chemical workstation (Lanlike, Tianjin China) in the range of 0.01-3 V at a scanning rate of 0.1 mV s^{-1}.

Results and discussion

The typical preparation process of porous ZMO-MSs could be briefly shown in Scheme 1. First, Mn^{2+} and Zn^{2+} react with CO_3^{2-} from the decomposition of urea at high temperature. Because of the same crystal structure, similar lattice constants and close solubility products of $ZnCO_3$ and $MnCO_3$, they would precipitate from the solution simultaneously and then form a solid solution, $Zn_xMn_{1-x}CO_3$. In order to minimize the surface energy [14,18,19], primary particles of $Zn_xMn_{1-x}CO_3$ aggregate together to form microspheres. After that, these microspheres are calcined at high temperature in air, resulting in the formation of $ZnMn_2O_4$. The releasing of CO_2 from carbonates makes the microspheres

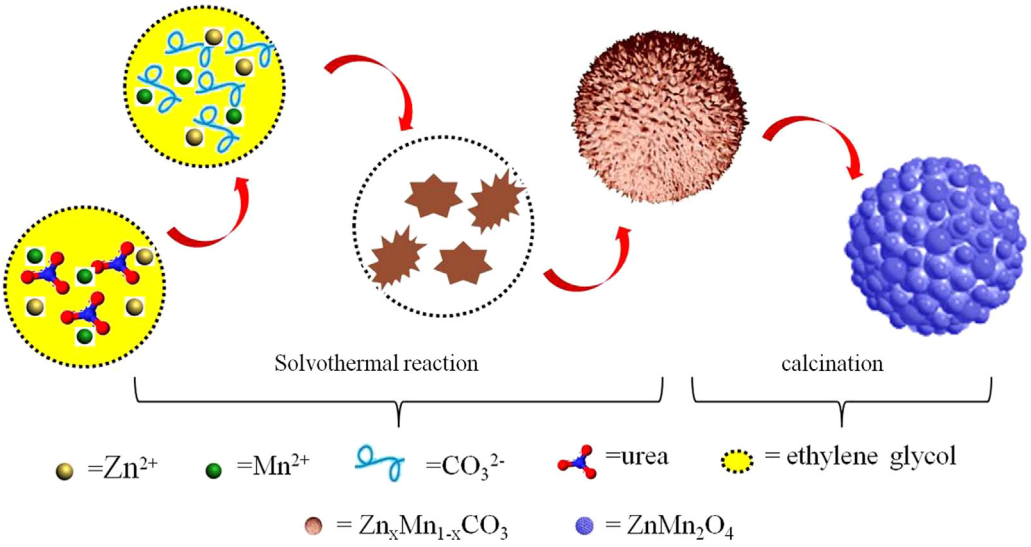

Scheme 1 Schematic illustration on the formation of porous $ZnMn_2O_4$ microspheres.

highly porous, which has been confirmed by SEM images and BET measurements.

As an important intermediate for porous ZMO-MSs, the product after the solvothermal reactions is characterized by XRD technique, SEM microscopy and FT-IR spectroscopy. As shown in Figure 1a, all the diffraction peaks could be attributed to a solid solution of $ZnCO_3$ (JCPDS Card, no. 08-0449) and $MnCO_3$ (JCPDS Card, no. 44-1472), which could be ascribed to their same crystal structure, close lattice constants and solubility products. The uniform mixture at an atomic level greatly benefits the formation of single-phase $ZnMn_2O_4$. No diffraction peaks belonging to oxides or hydroxides are detected in the XRD patterns. SEM image (Figure S1) shows that the product is dominated by uniform microspheres with their diameter around 2 μm, well consistent with Scheme 1. The formation of $Zn_xMn_{1-x}CO_3$ is also verified by FT-IR spectra (Figure S2). The sharp peaks at 726 and 864 cm^{-1} and the broad peak at 1385 cm^{-1} could be ascribed to in-plane bending, out-plane bending and asymmetric stretching of CO_3^{2-} [14,20]. The weak peaks at 2490, 2843 and 3391 cm^{-1} come from stretching vibration of C-H, symmetric stretching vibration of CH_2- and stretching vibration of O-H, which might be related with adsorbed organic species on the surface. This kind of adsorption is reasonable, in view of the synthesis in ethylene glycol [14].

The calcination of $Zn_xMn_{1-x}CO_3$ microspheres in air would result in the decomposition of metal carbonates and the formation of $ZnMn_2O_4$. The temperature is set at 600 °C, based on TGA curve of $Zn_xMn_{1-x}CO_3$ microspheres (Figure S3). As shown in Figure 1b, all the diffraction peaks after the calcination come from spinel-phase $ZnMn_2O_4$ (JCPDS Card, no. 24-1133). The narrow peak width and high peak intensity indicate the good crystallinity of $ZnMn_2O_4$, which is also supported by HRTEM images. The lattice constants calculated from this pattern are a=5.728 Å, c=9.245 Å, which are close to the reported ones [8]. The crystal size based on Scherrer equation, is approximately 21 nm.

SEM and TEM images are taken to disclose the morphology of the as-obtained $ZnMn_2O_4$. As shown in Figure 2a and b, the product is composed of relatively uniform microspheres with

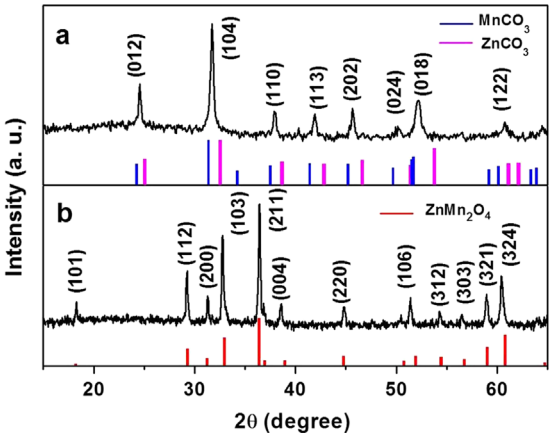

Figure 1 XRD patterns of (a) the product obtained after the solvothermal reaction, (b) the product after the calcination process.

an average diameter of 2 μm, almost the same as that of $Zn_xMn_{1-x}CO_3$ microspheres. This result indicates that most of each microsphere acts as a micro-reactor for the formation of ZMO. A close-up observation on a single microsphere (Figure 2c) reveals its unique surface structure that makes the microsphere look like an aggregate of many tiny particles. The neighboring particles connect together, creating a rough and porous microsphere. The porous feature of ZMO-MSs is also supported by TEM images. As illustrated in Figure 2d, the contrast difference caused by the porous feature could be still visualized, despite of its big size. Figure 2e confirms the granular feature of the ZMO-MSs surface. The particle size on the surface is around 20 nm, consistent with that obtained from Scherrer equation. HRTEM image gives clear lattice fringes with its spacing about 0.47 nm, corresponding to {101} planes of spinel-phase $ZnMn_2O_4$. Element mapping (Figure 2f) shows the uniform distribution of Zn and Mn in porous microspheres, which is in good agreement with $ZnMn_2O_4$. ICP-AES technique further gives the atomic ratio of Zn/Mn at 1:2, consistent with the stoichiometry of $ZnMn_2O_4$.

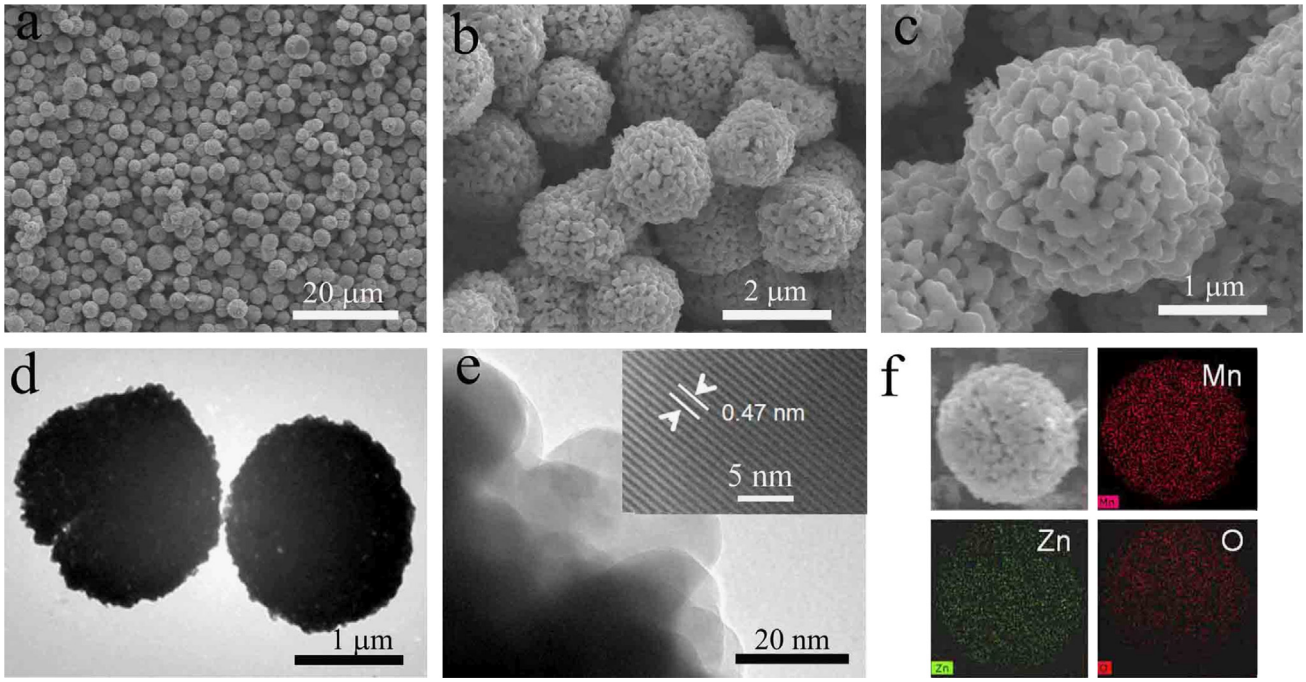

Figure 2 Low and high magnification SEM (a-c) images, TEM images (d), HRTEM image (e) and EDX mapping SEM images (f) of porous $ZnMn_2O_4$ microspheres.

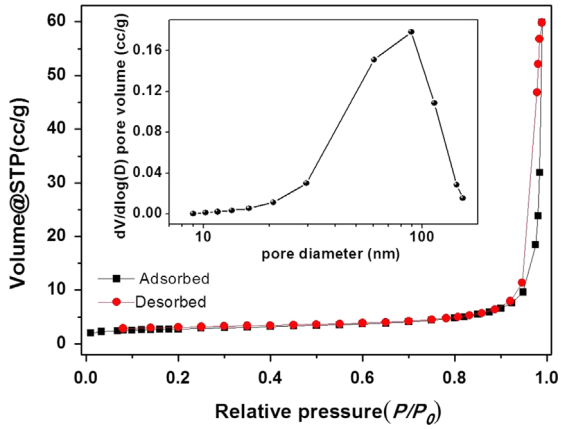

Figure 3 N_2 adsorption/desorption isotherm of porous $ZnMn_2O_4$ microspheres at 77 K and their pore size distribution curve (inset).

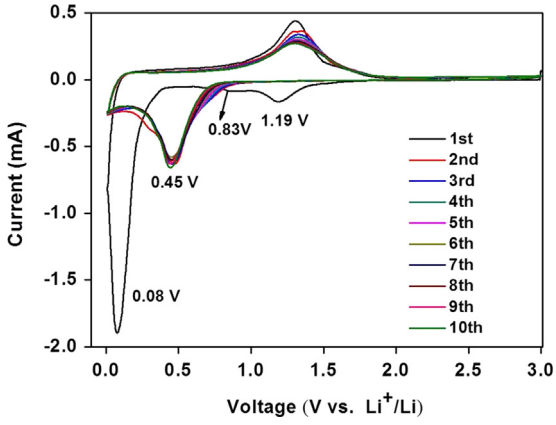

Figure 4 Cyclic voltammograms of the $ZnMn_2O_4$ sample at a rate of 0.1 mV s^{-1} in the voltage of 0.01-3.0 V vs. Li/Li^+.

The porous feature of ZMO-MSs is also confirmed by N_2 absorption-desorption measurements at 77 K. As shown in Figure 3, the N_2 sorption isotherm exhibits a typical TYPE-II profile, which is the characteristic of macroporous materials [11,21]. Based on Brunauer-Emmett-Teller (BET) model, the surface area and pore volume of ZMO-MSs are 17.7 m^2 g^{-1} and 0.27 cm^3 g^{-1}, respectively. The derived pore-size distribution indicates that the majority of the pores are in the range of 45-90 nm. Such a porous structure would effectively promote lithium storage, because it greatly enhances the diffusion of electrolyte to active materials and accommodate the volume variation during discharge/charge processes [22-24].

The electrochemical properties of porous ZMO-MSs are examined by cyclic voltammograms (CVs) with lithium foil as a reference and counter electrode. Figure 4 shows CVs of porous ZMO-MSs for the 1st, 2nd, 3rd and 10th cycle. During the first cathodic scan, the broad peak centered at 1.19 V, which vanishes in the following scans, could assign to the reduction of Mn^{3+} to Mn^{2+} [6,8]. The weak peak at 0.83 V might be related to the formation of solid electrolyte interphase (SEI) on the surface of porous ZMO-MSs because of the irreversible decomposition of the electrolyte [25,26]. The intense and broad peak located at 0.08 V corresponds to the reduction of Mn^{2+} to Mn^0 and Zn^{2+} to Zn^0 in Li_2O matrix, and the formation of Li-Zn alloy [7,27,28]. The reverse scan is featured by two peaks at 1.2 and 1.5 V, which could be associated with the oxidation of Mn to MnO and Zn to ZnO along with the decomposition of Li_2O matrix [29-31]. During the second cycle, the intense cathodic peak

moves to 0.45 V, which could be ascribed to the reduction of MnO and ZnO. After that, the subsequent CVs keep as almost the same, indicating the high electrochemical reversibility.

Figure 5a shows the discharge-charge curves of the porous ZMO-MSs at a current density of 100 mA g^{-1} in the range of 0.01-3.0 V (vs. Li^+/Li). The first discharge process of the porous ZMO-MSs exhibits two obvious plateaus between 0.01 and 3.00 V. The first plateau at 1.29 V is due to the reduction of Mn^{3+} to Mn^{2+}. The second plateau at 0.41 V corresponds to the formation of Mn^0, Zn^0 and Li-Zn alloy. The initial discharge capacity of porous ZMO-MSs is 1718 mAh g^{-1}, which is higher than the theoretical values (1024 mAh g^{-1}) based on the reaction ($ZnMn_2O_4 + 9Li^+ + 9e \rightarrow ZnLi + 2Mn + 4Li_2O$) [8,32]. The excess capacity may come from the formation of SEI film on the surface of active materials, lithium-insertion reaction in acetylene black and interfacial storage [24,33,34]. The initial charge capacity of porous ZMO-MSs is 1090 mAh g^{-1}, resulting in a coulombic efficiency of 63.4% for the first cycle. The large irreversible capacity of the first cycle can be attributed to the irreversible reactions related to SEI film, incomplete oxidation of Mn and Zn, and other side reactions [2,16,17,35]. The coulombic efficiency of the ZMO-MSs electrode increases to 96% for the second cycle and stabilizes above 99% after the fifth cycle, indicating good reversibility of the electrode.

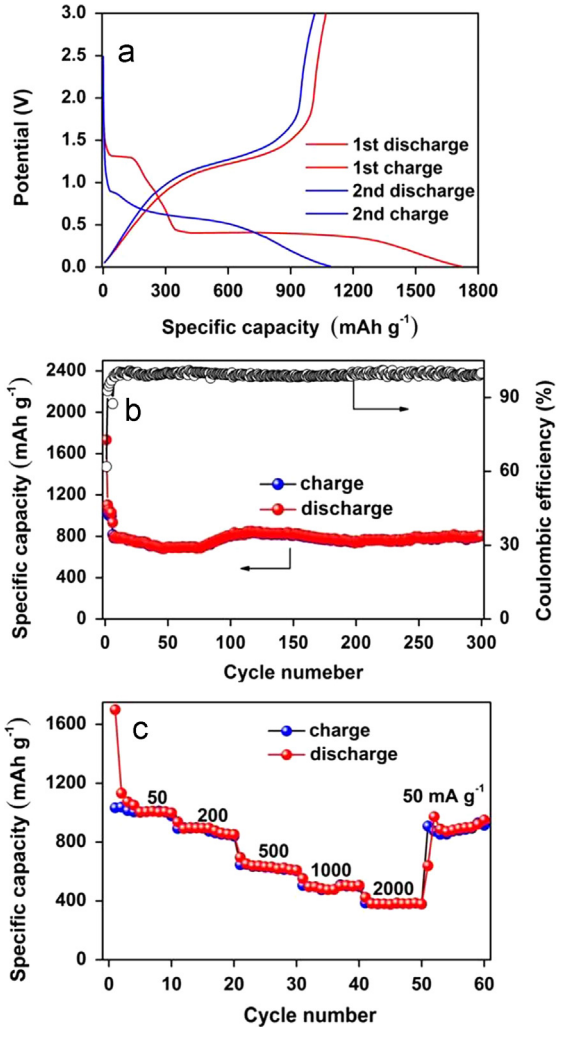

Figure 5 (a) The initial charge-discharge profiles of porous $ZnMn_2O_4$ microspheres at a current density of 100 mA g^{-1} over 0.01-3.0 V. (b) Cycling performance and coulombic efficiency of porous $ZnMn_2O_4$ microspheres at a current density of 500 mA g^{-1}. (c) Rate performance of porous $ZnMn_2O_4$ microspheres.

In Figure 5b, the cycling performance of the porous ZMO-MSs is presented in 0.01-3 V at a current density of 500 mA g^{-1}. The specific capacity slowly decreases to 700 mAh g^{-1} after the first 50 cycles, which has been observed in many transition metal oxides [8,34,36-38]. Afterwards, the specific capacity gradually increases to 800 mAh g^{-1} until 100th cycle. Finally, the electrode keeps a specific capacity of 800 mAh g^{-1} even after 300 cycles, which is better than most of the reported $ZnMn_2O_4$ nanomaterials. For example, $ZnMn_2O_4$ nanocrystallites with their size over 30-60 nm exhibited a reversible capacity about 569 mAh g^{-1} at 100 mA g^{-1} after 50 cycles [8]. Although the reversible capacity could be enhanced to 650 mAh g^{-1} by $ZnMn_2O_4$ nanowires [9], it is still lower than our case. The specific capacity of $ZnMn_2O_4$ nanoplate assemblies is even worse, only 502 mAh g^{-1} at 60 mA g^{-1} over 30 cycles [10]. Compared with these results, that of hollow microspheres rises to 750 mAh g^{-1} at a rate of 400 mA g^{-1} after 120 cycles [12].

The excellent cycling performance of the ZMO-MSs could be attributed to the interconnected porous structure. The internal pores can be flooded with electrolyte, providing good accesses of the electrolyte to the electrode surface. Large surface area between these particles facilitates charge transfer and the short diffusion distance of Li^+ [15-17,35]. Moreover, the porous structure can accommodate volume change during the repeated Li^+ insertion/extraction, thus alleviating the pulverization problem [15,16]. As presented in Figure 6, the porous ZMO-MSs basically preserve their morphology and surface feature after 50 cycles at 500 mA g^{-1}, which confirms the morphology and surface stability again.

The high rate capability of porous ZMO-MSs is also measured. As shown in Figure 5c, the porous ZMO-MSs give the specific capacities of 1050, 896, 654, 496 and 395 mAh g^{-1} at the current densities of 50, 200, 500, 1000, 2000 mA g^{-1}. Even at a high current density of 2 A g^{-1}, the capacity is still higher than the theoretical capacity of graphite (372 mAh g^{-1}). The rate performance of porous ZMO-MSs is better than previous works. For example, ball-in-ball hollow $ZnMn_2O_4$ microspheres maintained a specific capacity of 396 mAh g^{-1} at a current density of 1200 mA g^{-1} [12]. Hollow $ZnMn_2O_4$ microspheres delivered 361 mAh g^{-1} at a current density of 1600 mA g^{-1} [11]. As the current density is back to 50 mA g^{-1}, the capacity of around 1000 mAh g^{-1} can be retrieved, suggesting good structure stability of the active material.

Conclusion

In summary, porous ZMO-MSs are successfully synthesized by calcination of metal carbonates prepared by a solvothermal reaction. XRD patterns, SEM images, TEM/HRTEM images and N_2 adsorption/desorption isotherm reveal the good crystallinity and porous feature of spinel-phase ZMO-MSs. Their performance as an anode material shows a specific capacity of 800 mAh g^{-1} after 300 cycles at a current

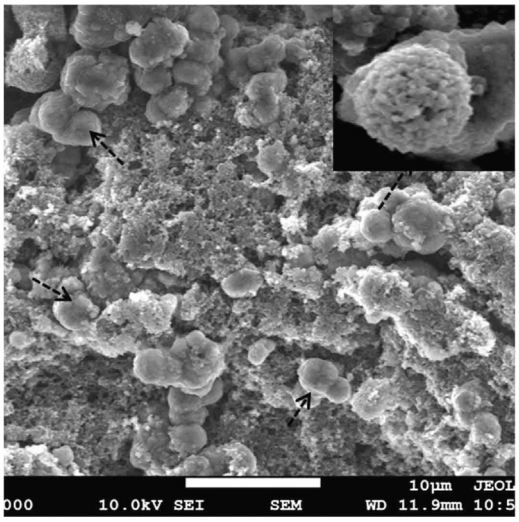

Figure 6 SEM image of the electrode based on porous $ZnMn_2O_4$ microspheres after 50 cycles at 500 mA g^{-1}.

density of 500 mA g^{-1}. At 2 A g^{-1}, the reversible capacity could be 395 mAh g^{-1}, still higher than the theoretical capacity of graphite. The good cycling stability and rate capability could be ascribed to the unique structure where porous microspheres are composed by tiny nanoparticles.

Acknowledgments

This work was supported by the 973 Project of China (No. 2011CB935901), National Natural Science Foundation of China (Nos. 91022033, 51172076, 21203111), New Century Excellent Talents in University (NCET-10-0369), Shandong Provincial Natural Science Foundation for Distinguished Young Scholar (JQ201205), Independent Innovation Foundations of Shandong University (2012ZD007), and New-faculty Start-up Funding in Shandong University (No. 20111017).

Appendix A. Supporting information

Supplementary data associated with this article can be found in the online version at http://dx.doi.org/10.1016/j.nanoen.2014.04.001.

References

[1] M. Armand, J.M. Tarascon, Nature 451 (2008) 652–657.
[2] P.G. Bruce, B. Scrosati, J.M. Tarascon, Angew. Chem. Int. Ed. 47 (2008) 2930–2946.
[3] J.M. Tarascon, M. Armand, Nature 414 (2001) 359–367.
[4] J.F. Li, S.L. Xiong, X.W. Li, Y.T. Qian, J. Mater. Chem. 22 (2012) 23254–23259.
[5] S.H. Choi, Y.C. Kang, ChemSusChem 6 (2013) 2111–2116.
[6] Z.C. Bai, N. Fan, C.H. Chang, Z.C. Ju, C.L. Guo, J. Yang, Y.T. Qian, Nanoscale 5 (2013) 2442–2447.
[7] X.W. Guo, X. Lu, X.P. Fang, Y. Mao, Z.X. Wang, L.Q. Chen, X.X. Xu, H. Yang, Y.N. Liu, Electrochem. Commun. 12 (2010) 847–850.
[8] Y.Y. Yang, Y.Q. Zhao, L.F. Xiao, L.Z. Zhang, Electrochem. Commun. 10 (2008) 1117–1120.
[9] S.W. Kim, H.W. Lee, P. Muralidharan, D.H. Seo, W.S. Yoon, D.K. Kim, K. Kang, Nano Res. 4 (2011) 505–510.
[10] J. Zhao, F.Q. Wang, P.P. Su, M.R. Li, J. Chen, Q.H. Yang, C. Li, J. Mater. Chem. 22 (2012) 13328–13333.
[11] L. Zhou, H.B. Wu, T. Zhu, X.W Lou, J. Mater. Chem. 22 (2012) 827–829.
[12] G.Q. Zhang, L. Yu, H.B. Wu, H.E. Hoster, X.W Lou, Adv. Mater. 24 (2012) 4609–4613.
[13] F.M. Courtel, H. Duncan, Y. Abu-Lebdeh, I.J. Davidson, J. Mater. Chem. 21 (2011) 10206–10218.
[14] C.Z. Yuan, J.Y. Li, L.R. Hou, L.H. Zhang, X.G. Zhang, Part. Part. Syst. Charact. (2014). http://dx.doi.org/10.1002/ppsc.201300338.
[15] A. Vu, Y.Q. Qian, A. Stein, Adv. Energy Mater. 2 (2012) 1056–1085.
[16] Y. Li, Z.Y. Fu, B.L. Su, Adv. Funct. Mater. 22 (2012) 4634–4667.
[17] J. Maier, Angew. Chem. Int. Ed. 52 (2013) 4998–5026.
[18] H. Colfen, S. Mann, Angew. Chem. Int. Ed. 42 (2003) 2350–2365.
[19] H. Colfen, M. Antonietti, Angew. Chem. Int. Ed. 44 (2005) 5576–5591.
[20] L.Z. Wang, F.Q. Tang, K. Ozawa, Z.G. Chen, A. Mukherj, Y.C. Zhu, J. Zou, H.M. Cheng, G.Q. Lu, Angew. Chem. Int. Ed. 127 (2009) 7182–7185.
[21] M. Kruk, M. Jaroniec, Chem. Mater. 13 (2001) 3169–3183.
[22] N. Yan, L. Hu, Y. Li, Y. Wang, H. Zhong, X.Y. Hu, X.K. Kong, Q.W. Chen, J. Phys. Chem. C 116 (2012) 7227–7235.
[23] J.S. Xu, Y.J. Zhu, ACS Appl. Mater. Interfaces 4 (2012) 4752–4757.
[24] L. Hu, H. Zhong, X.R. Zheng, Y.M. Huang, P. Zhang, Q.W. Chen, Sci. Rep. 2 (2012) 986.
[25] Y. Cao, L. Xiao, X. Ai, H. Yang, Electrochem. Solid-State Lett. 6 (2003) A30–33.
[26] K.F. Zhong, X. Xia, B. Zhang, H. Li, Z.X. Wang, L.Q. Chen, J. Power Sources 195 (2010) 3300–3308.
[27] N.N. Wang, H.Y. Xu, L. Chen, X. Gu, J. Yang, Y.T. Qian, J. Power Sources 247 (2014) 163–169.
[28] H. Li, X.J. Huang, L.Q. Chen, Solid State Ion. 123 (1999) 189–197.
[29] D. Pasero, N. Reeves, A.R. West, J. Power Sources 141 (2005) 156–158.
[30] Y. Sharma, N. Sharma, G.V.S. Rao, B.V.R. Chowdari, Adv. Funct. Mater. 17 (2007) 2855–2861.
[31] Z. Xing, Z.C. Ju, J. Yang, H.Y. Xu, Y.T. Qian, Nano Res. 5 (2012) 477–485.
[32] Y.F. Deng, S.D. Tang, Q.M. Zhang, Z.C. Shi, L.T. Zhang, S. Z. Zhan, G.H. Chen, J. Mater. Chem. 21 (2011) 11987–11995.
[33] P. Balaya, H. Li, L. Kienle, J. Maier, Adv. Funct. Mater. 13 (2003) 621–625.
[34] W. Wei, S.B. Yang, H.X. Zhou, I. Lieberwirth, X.L. Feng, K. Müllen, Adv. Mater. 25 (2013) 2909–2914.
[35] Y. Wang, G.Z. Cao, Adv. Mater. 20 (2008) 2251–2269.
[36] L. Li, K.H. Seng, Z.X. Chen, Z.P. Guo, H.K. Liu, Nanoscale 5 (2013) 1922–1928.
[37] S. Grugeon, S. Laruelle, L. Dupont, J.-M. Tarascon, Solid State Sci. 5 (2003) 895–904.
[38] S. Laruelle, S. Grugeon, P. Poizot, M. Dolle, L. Dupont, J.M. Tarascon, J. Electrochem. Soc. 149 (2002) A627–A634.

Nana Wang received her B.S. degree from Hangzhou Normal University in 2011. Then, she joined Prof. Qian's group in July, 2011. Now she is a Ph.D. candidate in School of Chemistry and Chemical Engineering of Shandong University. Her research focuses on the synthesis of nanostructured transitional metal oxides as anode materials for lithium-ion batteries.

Xiaojian Ma received her Ph.D. degree in School of Chemistry and Chemical Engineering, Shandong University in 2013. Now she works in Shandong University. She is interested in the controllable synthesis of novel silicon carbide nanomaterials.

Huayun Xu is an assistant professor of chemistry at School of Chemistry and Chemical Engineering, Shandong University. She was awarded her B.S. degree from Qingdao University, in 2002 and Ph.D. degree from University of Science and Technology of China (USTC) in 2007. After that, she moved to Shandong University of Science and Technology from 2007 to 2010. During 2008–2009, she worked at Chonnam National University in South Korea as a post doctor. Her current interests concentrate on the development of novel electrode materials for advanced lithium-ion batteries and sodium-ion batteries.

Liang Chen got his B.S. degree from Lanzhou University in 2010. He is currently a Ph.D. candidate in School of Chemistry and Chemical Engineering, Shandong University. He is especially interested in the rational design of vandium oxides as cathode materials for lithium ion batteries.

Jie Yue is a graduate student in School of Chemistry and Chemical Engineering, Shandong University. She received her B.S. degree from Qufu Normal University in 2012. Then, she came to Shandong University as a graduate student. She is interested in Mn-related anode materials for lithium ion batteries.

Feier Niu is a graduate student in School of Chemistry and Chemical Engineering, Shandong University. She got her B.S. degree from Shandong Normal University, China, in 2013. After joined in Prof. Qian's group, she shows intense interests in lithium-air battery.

Jian Yang is a QiLu professorship in chemistry at School of Chemistry and Chemical Engineering, Shandong University. He received his Ph.D. degree from University of Science and Technology of China, in 2002. Then, he worked as a postdoctor in National Taiwan Normal University, Singapore-MIT alliance, University of Washington (Seattle) from 2002 to 2007. In 2007, he is back to china in South China University of Technology in Guangzhou as a full professor. He moved to Shandong University in 2011. His research interests include the formation mechanism underneath the synthesis of novel nanomaterials, and their applications in lithium-ion batteries, sodium-ion batteries, etc.

Yitai Qian received his B.S. degree in chemistry from Shandong University in 1962. He was selected as an academician of Chinese Academy of Sciences in 1997. He presently is a Professor of University of Science and Technology of China, and he is also the director of the Key Laboratory of Colloid and Interface Chemistry (Shandong University), Ministry of Education. In 2008, he became a Fellow of the RSC. Professor Qian has published more than 800 refereed journal publications and several invited book chapters. He has active research programs in solid state chemistry, especially on the synthesis of nanomaterials.